RESEARCH ARTICLE

Macro-
molecular
Materials and Engineering
Open Access

www.mame-journal.de

Perpendicular Alignment of 2D Nanoplatelet Emitters in Electrospun Fibers: A Result of the Barus Effect?

Xu Liu, Fuzhao Li, Manuel Hohgardt, Lars Frederik Klepzig, Marcel Maximilian Willich, Henrik-Alexander Christ, Andreas Schaate, Peter Behrens, Jannika Lauth,* Henning Menzel,* and Peter Jomo Walla*

Stable jet electrospinning (SJES) is a special form of optical fiber generation that prevents chaotic fiber whipping typical for conventional electrospinning procedures. Incorporation of highly emissive semiconductor nanoplatelets (NPLs) in such fibers has very high potential in optical data transmission, optological circuits, fiber lasers, solar light concentrators and many other fields because NPLs exhibit strongly directed emission from their surface plane due to various in-plane transition dipole moments. However, potential orientation control of 2D-NPLs in SJES is entirely unknown as electric fields and various mechanical forces contribute in a complex manner simultaneously. Here, the observation of counter-intuitive yet very beneficial orientation of rectangular CdSe/CdS 2D-NLP in SJES perpendicular to the fiber drawing axis is reported. Scanning electron microscopy, 3D-single particle excitation polarization microscopy, 3D-photogoniometry, polarized emission spectroscopy and small angle X-ray scattering (SAXS) demonstrate aggregation free perpendicular alignment of the NPLs in poly(methyl methacrylate) (PMMA) fibers, resulting in dominant emission in directions parallel to the fiber. It is suggested that the observed vertical alignment is due to normal forces resulting from viscoelastic expansion when the polymer solution leaves the cannula (Barus effect) and that using such perpendicular nano-emitter alignment forces allows for the generation of novel materials also beyond fibers.

1. Introduction

Emissive nanomaterials come in many different shapes and sizes, defining the anisotropic radiation patterns and wavelengths, and are typically much more stable than conventional organic dyes. Therefore, alignment of nanometric light sources with anisotropic radiation patterns fundamentally opens a wide range of entirely new applications. Among these nanometric light-sources, 2D semiconductor nanoplatelets (NPLs) exhibit particular and fundamentally interesting emission patterns. In comparison to conventional organic dyes and rod- and sphere like nanoparticles – that all have either single transition dipole moment (TDM) (**Figure** 1h) or isotropic radiation emission patterns – the in-plane dipole distribution of NPLs results in directional emission perpendicular to the platelet plane (Figure 1i)[1–4] Owing to the special absorption and emission radiation pattern, highly aligned NPLs can absorb light from most angles and redirect it into desired directions. [5–8] Such a controlled emission of individual NPLs will

X. Liu, M. Hohgardt, M. M. Willich, P. J. Walla
Department for Biophysical Chemistry, Institute of Physical and Theoretical Chemistry
Technical University of Braunschweig
38106 Braunschweig, Germany
E-mail: p.walla@tu-braunschweig.de

F. Li, H.-A. Christ, H. Menzel
Department for Macromolecular Chemistry, Institute of Technical Chemistry
Technical University of Braunschweig
38106 Braunschweig, Germany
E-mail: h.menzel@tu-braunschweig.de

The ORCID identification number(s) for the author(s) of this article can be found under https://doi.org/10.1002/mame.202300027

© 2023 The Authors. Macromolecular Materials and Engineering published by Wiley-VCH GmbH. This is an open access article under the terms of the Creative Commons Attribution License, which permits use, distribution and reproduction in any medium, provided the original work is properly cited.

DOI: 10.1002/mame.202300027

L. F. Klepzig, J. Lauth
Institute of Physical Chemistry and Electrochemistry
Leibniz University Hannover
30167 Hannover, Germany
E-mail: jannika.lauth@pci.uni-hannover.de

A. Schaate, P. Behrens
Department for Inorganic Solid-State and Materials Chemistry, Institute of Inorganic Chemistry
Leibniz University Hannover
30167 Hannover, Germany

J. Lauth
Institute of Physical and Theoretical Chemistry
University of Tübingen
72076 Tübingen, Germany

P. J. Walla
Group Biomolecular Spectroscopy and Single Molecule Detection
Max-Planck Institute for Multidisciplinary Sciences
37077 Göttingen, Germany

X. Liu, F. Li, L. F. Klepzig, A. Schaate, P. Behrens, J. Lauth, H. Menzel, P. J. Walla
Cluster of Excellence PhoenixD (Photonics, Optics and Engineering – Innovation Across Disciplines)
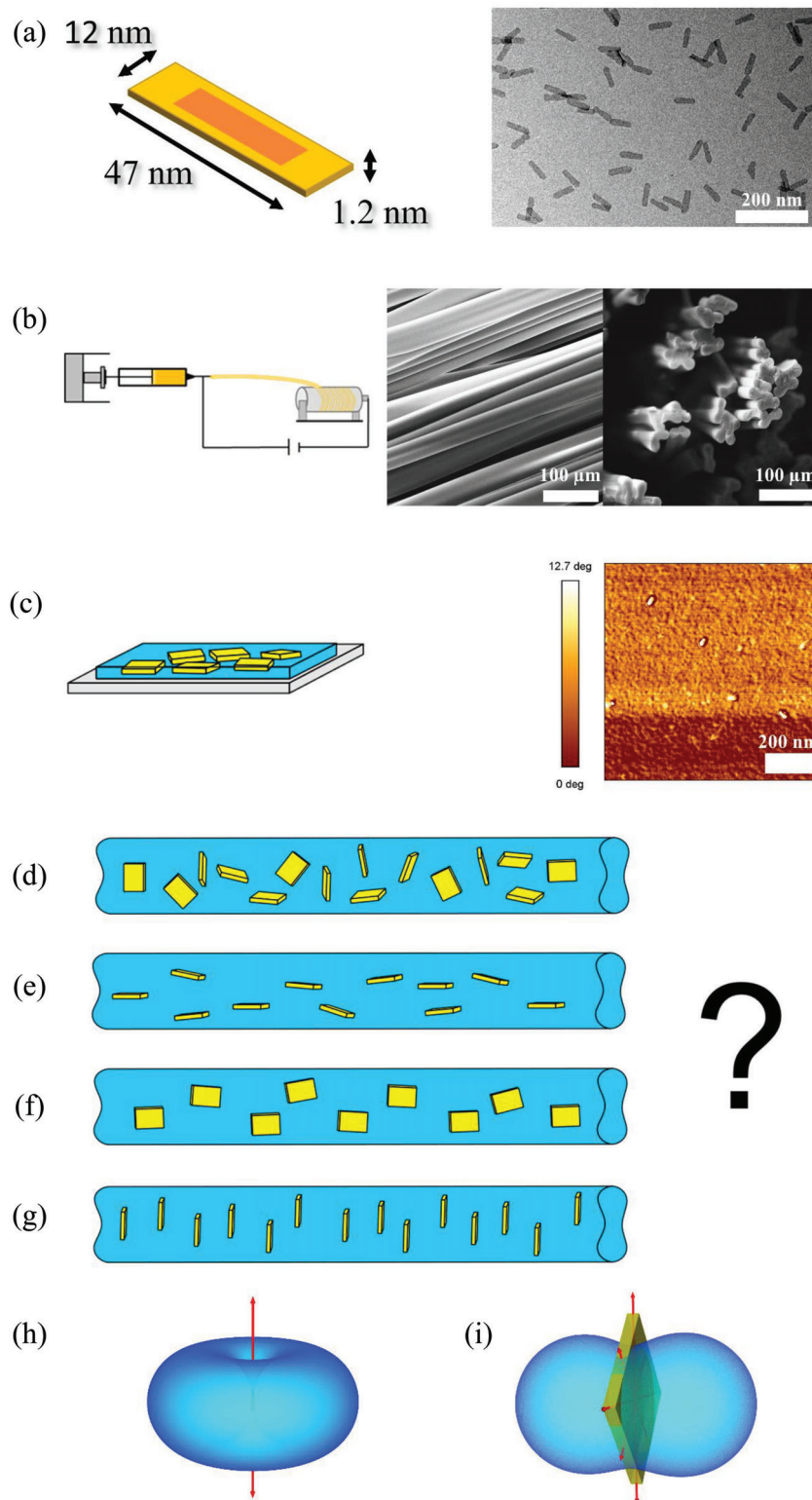30167 Hannover, Germany

ADVANCED
SCIENCE NEWS

www.advancedsciencenews.com

{M} acro-
olecular
Materials and Engineering
Open Access

www.mame-journal.de

Figure 1. a) Composition and dimensions of 2D CdSe/CdS NPLs along with a representative TEM image. b) Schematic representation of the stable jet electrospinning process along with SEM images showing the smooth surface and the ribbon like ("dog-bone" shaped) cross section of the fibers. c) Schematic illustration of polymer/NPL nanocomposite control samples with NPLs deposited parallel to the surface of a microscopic cover slip by the layer-by-layer method along with a corresponding AFM image of the NPLs on the cover slip. d–g) Schematic representation of potential distributions of the NPLs in the electrospun fibers. h) Radiation pattern (blue) of a single dye with a certain transition dipole moment orientation (red) and i) radiation pattern (blue) of a single NPL (yellow) with a distribution of transition dipoles (red) in the plane.

**ADVANCED
SCIENCE NEWS**

www.advancedsciencenews.com

Macro-
molecular
Materials and Engineering
Open Access

www.mame-journal.de

allow nanometric optological circuits based on exchange of photons and excitons in predefined directions, directing and concentrating diffusively scattered solar light onto photovoltaics and many other new applications in fields such as display technology, fiber lasers, or optical telecommunication.[7,9–18] From a fundamental point of view, partial refocusing of scattered light is impossible with conventional optics such as lenses or mirrors but is possible with aligned NPLs and raises interesting questions to what extend such scattered light refocusing is possible in accordance with the second law of thermodynamics.[19]

However, inorganic NPLs are usually randomly dispersed in organic bulk solution and aggregation can easily occur during a fabrication process. Even though examples of NPLs aligned in aggregated cluster structures exist, the aggregation free alignment of nanoparticles that are at least to some extend isolated from each other has so far proven to be basically impossible on larger scales.[20–26] This, however, is of fundamental importance as many of the beneficial optical characteristics are drastically reduced as soon as the NPLs aggregate or come closer together. For example, highest emission quantum efficiencies close to 100% could only be observed from well isolated NPLs and also the anisotropic emission patterns and spectral characteristics are often severely compromised by aggregation.[22,24,25] Therefore, the necessary alignment of NPLs in larger volumes and at sufficient distances remained to be a big challenge.

Electrospinning is one of the few techniques that is able to produce continuous ultrafine fibers with diameters ranging from a few micrometers to tens of nanometers.[27–29] With the increasing importance of fibers in optics and photonics, electrospinning provides a straight-forward possibility to produce functional optical materials by incorporating dye molecules or inorganic light emitters such as NPLs into the polymer solution.[30,31] Typically, the fibers are collected as disordered nonwoven, however, by changing the process parameters, a special mode called stable jet electrospinning (SJES) can be achieved to produce aligned fibers for optical applications such as waveguides.[32–35]

Here, we report on embedding of anisotropically photoluminescent 2D CdSe/CdS NPLs into Poly(methyl methacrylate) (PMMA) fibers by SJES which results in counter-intuitive but very beneficial NPL orientation perpendicular to the fiber direction. Highly aligned hybrid fibers with different loadings of NPLs were prepared. Scanning electron microscopy, 3D-single particle excitation polarization microscopy, 3D-photogoniometry, and polarized emission spectroscopy confirmed aggregation free orientation of NPLs perpendicular to the fiber direction and dominant anisotropic emission parallel to the optical axis of the fibers. Therefore, the vast majority of the light emitted by the NPLs will stay within the fibers by waveguiding. This can be used to direct the light very specifically into any desired direction even if the light was entirely diffusive or scattered before the absorption through the NPLs. Reasons for this counter intuitive perpendicular alignment of the NPLs are discussed. We suggest the stretching of the polymer coils due to flow in the cannula and their viscoelastic relaxation at the exit (Barus effect) is leading to orientational forces perpendicular to the spinning direction. This principle allows the generation of an entire new range of advanced materials by using such forces to exactly align nano-emitters as desired when flows and restrictive wall forces are correspondingly designed.

2. Results

The dimensions of the 2D CdSe/CdS NPLs and the NPL containing fibers prepared by SJES are schematically illustrated in Figure 1a,b. Details of the core-crown CdSe/CdS NPL synthesis are described in the Materials and Methods section. The 2D NPLs had a well-defined and monodisperse thickness of 4 monolayers (4 layers of Se, 5 layers of Cd) resulting in narrow photoluminescence at 512 nm (2.42 eV) with a FWHM of 8.2 nm (38 meV).[36]

Electrospinning is a process based on electrostatic drawing of a polymer solution droplet into an initially linear liquid stream (jet).[28] For this, a high electrical potential is typically applied between a spinneret and a nearby collector (Figure 1b). Usually, the electrostatic drawing forces in combination with emerging bending instabilities lead to a chaotic whipping phenomenon that further elongates the jet. The chaotic whipping results in the very thin fibers being collected as a nonwoven without specific orientation of the fiber directions.[28] Unsurprisingly, CdSe/CdS core-shell NPLs in chaotically woven fibers lack any specific NPLs orientation.[37]

However, in the so-called SJES the chaotic whipping of the jet is suppressed.[35] Here, the bending instabilities of the jet that would lead to chaotic whipping in traditional electrospinning are suppressed by high viscoelasticity and chain entanglement of the polymers in the spinning solution which leads to the highly aligned somewhat thicker microfibers.[38,39] We have used PMMA in 2-butanone at a concentration of 35 wt.% and an electric field of 35 kV to reach the stable jet regime (for details see Experimental Section). We decided to use PMMA as polymer because it tends to have very smooth surfaces which is important for many optical applications. In addition, it is known to be a very stable polymer. Indeed, the SEM images in Figure 1b demonstrate that the fibers prepared in this way have a smooth surface and a "dog bone" shaped cross section. This more ribbon like cross section is often observed for highly viscous solutions and thicker fibers and can be attributed to a slow drying of the fiber from the outside in and is not dependent on the cannula shape.[40] However, independent of the cross-sectional shape, a smooth surface is an important requirement for fibers suitability as light wave guides, for example, in fiber laser or telecommunication applications.

To characterize the emission and absorption of single NPLs with known orientation, a sample of polymer/NPL nanocomposites with the NPLs oriented parallel to the surface of a microscope cover slip was prepared by layer-by-layer deposition.[41] This sample was used as a control and the orientation was reconfirmed by AFM (Figure 1c, for details see Experimental Section).

While it is clear that the orientation of the NPLs on the coverslips is uniformly parallel to substrate surface, nothing was known about the orientation of the nanoplates embedded in the fibers after the electrospinning process. It could be expected that they either stay randomly oriented (Figure 1d) during electrospinning or are in some way aligned during this process, for example parallel to the spinning direction (Figure 1e, f) or perpendicular to it (Figure 1g). It turned out that the intuitive idea of determining the orientation with TEM measurements cannot be implemented due to the 3D distribution of the NPLs in the entire fibers and the relatively low concentration. Either none or only one NPL is expected in TEM images. In addition, slicing of PMMA is

intrinsically hindered by effects such as bloating. Therefore, we applied various emission and excitation polarization and anisotropy methods that are sensitive to the orientation of the platelets including microscopic observation of the 3D orientations of hundreds of single NPLs within the fibers. These measurements are best suited to detect a statistically significant number of hundreds of NPL positions and orientations in one image simultaneously together with the full fiber direction image itself.[37]

In order to understand the excitation and emission anisotropy of NPLs, it is important to know that compared to organic dye molecules, the NPLs do not have one single, discrete TDM, but rather a distribution of TDMs within their plane.[2,6] For comparison, Figure 1h illustrates the orientation of the transition dipole moment (red arrow) of a single fluorescence dye and the corresponding emission radiation pattern (blue donut shaped distribution). In excitation experiments, the probability to excite the molecule and thus observe emission from it is the highest, when the polarization vector of the exciting light is parallel to the TDM (red). Since the TDMs of NPLs are oriented isotropically within the plane (as indicated by the red arrows in Figure 1i), their excitation is equally well possible with exciting light polarization vectors in different directions. Still, the probability to excite the NPLs is the highest when the polarization vector of the exciting light is parallel to any of these vectors and lowest when it is perpendicular to the plane of the NPLs. In addition, the sum of the donut shaped radiation pattern from all dipole moment orientations within the plane of an NPL averages to a dumbbell shaped radiation pattern as indicated in Figure 1i (blue distribution).[2]

Previously it has been reported that the radiation pattern is still circularly symmetric perpendicular to the plane of 2D CdSe NPLs (Figure 1i) even when the platelets are rectangularly shaped (Figure 1a) and is not distorted in the direction of the long axis of the platelets (for example as illustrated in Figure 1, Supporting Information).[2] As this is important for further characterization of the NPLs' orientation, we first examined if this is also the case with the rectangular CdSe/CdS core-crown NPLs used in this study. To check this, a bilayer of polymer/NPLs nanocomposite aligned parallel to the coverslip surface (Figure 1c) was examined using 3D-single particle excitation polarization microscopy (**Figure 2**a-d). 3D-single particle excitation polarization microscopy allows to determine 3D TDM-orientations of the individual NPL by recording the NPL-emission intensities in a microscope set-up as a function exciting light polarizations and directions varying in multiple 3D orientations.[9,10] First, the NPLs in the nanocomposite film were excited at angles of 35° from three different directions with rotating excitation polarization (Figure 2b) and the emission intensities of individual NPLs were recorded. The observation of the nearly identical polarization-dependent intensity patterns with all three directions (Figure 2b) confirms that there is no dependence on the excitation direction of the rectangular NPLs and that the excitation probability is the same in each case (measurements in Figure 2b are exemplarily shown for the white encircled NPL in Figure 2d). Very similar signals were observed from all individual NPLs as they are all oriented flat in the nanocomposite film. When single NPLs were illuminated directly from below (Figure 2c), again by rotating the excitation beam polarization, almost no intensity variations were observed. This demonstrates that excitation probability is nearly

circularly symmetric perpendicular to the plane of the rectangular NPLs, i.e., confirming the pattern shown in Figure 1i also for our rectangular NPLs. Again, very similar signals were observed from all individual NPLs.

Next, individual NPLs in the electrospun fibers (0.03 wt.% with respect to PMMA) were explored in the 3D-single particle excitation polarization microscope (Figure 2e-i). The amplitude of the intensity modulation observed with rotating excitation polarization differed significantly when using the three different excitation directions (Figure 2f). With the excitation direction perpendicular to the fiber (Figure 2f, left) the intensity modulation was the highest while the other two directions had significantly lower modulation amplitudes. With the excitation direction perpendicular to the fiber (Figure 2f, left), the excitation was highest when the polarization was perpendicular to the fibers whereas it was lowest when it was parallel (as illustrated by the double arrows on the left in Figure 2f). Therefore, a random distribution of nanoparticle orientations such as illustrated in Figure 1d as well as a planar distribution such as illustrated in Figure 1f and as seen in Figure 2a,b can be excluded. As the observed intensity in Figure 2f (left) was lowest, when the excitation polarization was parallel to the fibers, an alignment such as illustrated in Figure 1e ("in-line" with fiber axis) can also be excluded – if the NPLs would be aligned parallel to the fiber direction, the highest excitation probability would occur with a polarization parallel to the fibers. However, the highest excitation probability occurred with a polarization perpendicular to the fibers, demonstrating the NPLs are actually oriented perpendicularly to the fiber direction.

In order to explore the angle distribution of the perpendicular alignment of the NPLs in more detail, we determined the orientation of many individual NPLs (Figure 2g–i). With a distinct fiber orientation, the normalized raw data of many individual NPLs in the fiber were very similar in phase (Figure 2g). From the variations in the phase of the intensity modulation from each nanoplatelet and excitation direction, the 3D-orientation of each NPL is calculated and the histogram of all observed orientations projected onto the plane parallel to the microscope objectives surface is shown in the polar plot in Figure 2i. This histogram shows a dominant orientation of all platelets (red line in Figure 2i) perpendicular to the fiber direction (blue line in Figure 2i) and provides additional information about the actual angle distribution of the NPL alignment.

Figure 3a shows more electrospun fibers with different orientations relative to the three excitation directions in our microscope along with the histograms of the NPL orientation projections in the plane of the microscope surface. The data from the fibers observed at angles of -5°, 52°, and 150° confirm that the NPLs are arranged preferably at angles perpendicular to the direction of the fibers with average orientations and angle distributions of 83±21°, 131±12°, and 243±17°, respectively.

While 3D-single particle excitation polarization microscopy is based on analyzing different excitation probabilities observed with different angles of the excitation polarization vectors relative to the TDMs (red arrows in Figure 1i), polarized emission spectroscopy also considers differences in the emission polarization observed with different orientations of the NPLs. For polarized emission spectroscopy, fibers with different orientations were recorded with excitation polarization and emission detection polarization being either parallel or perpendicular to the fiber
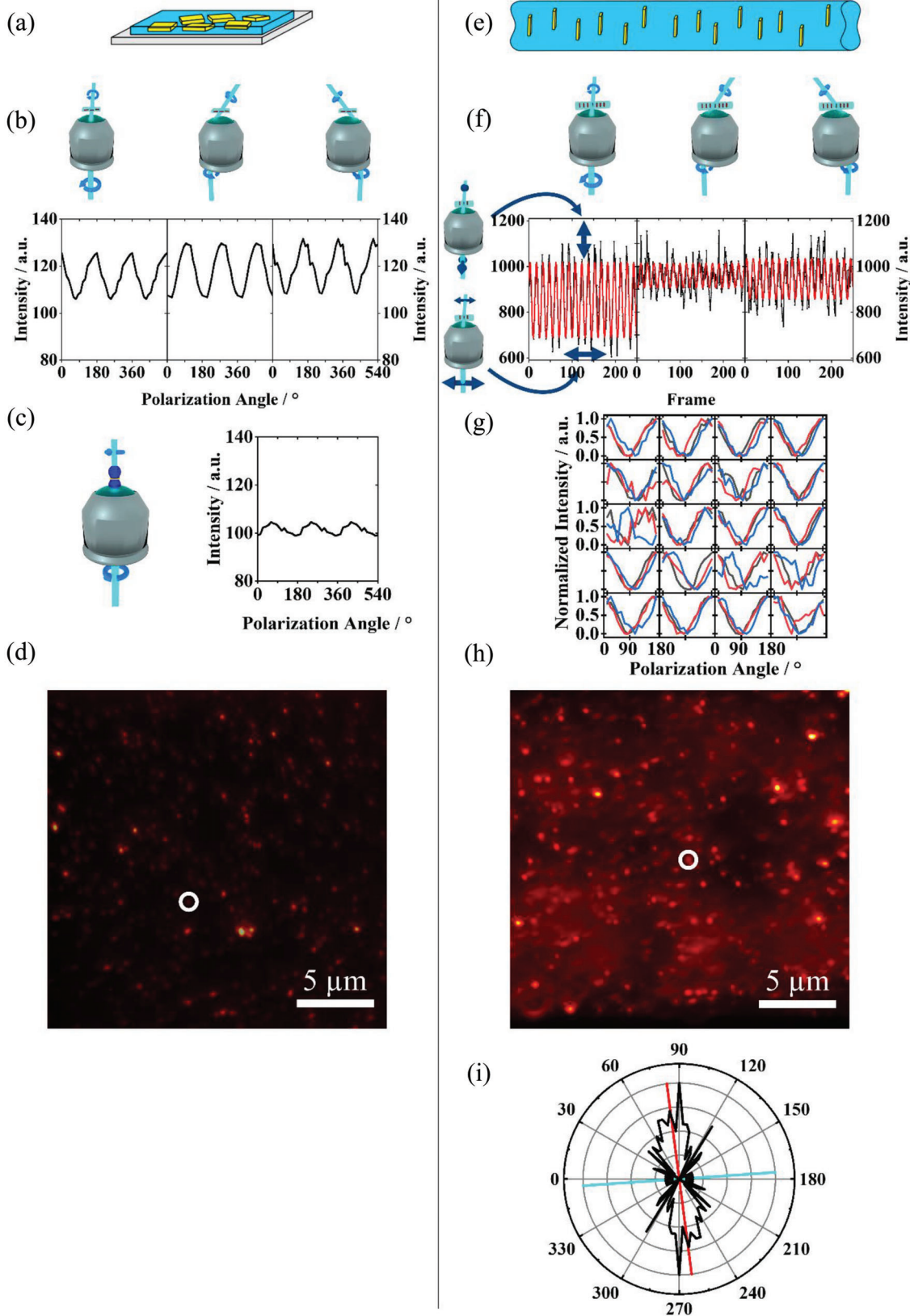
**ADVANCED
SCIENCE NEWS**

www.advancedsciencenews.com

**[M] acro-
olecular
Materials and Engineering**
Open Access

www.mame-journal.de

Figure 2. a) Illustration of nanocomposite control samples with NPLs parallel to the surface of a microscopes observation plane. b) Illustration of single NPL measurements with rotating polarization of the excitation light (light blue) from three different directions tilted by 35° along with the corresponding intensity variations experimentally observed from a single NPL encircled in (d). For details see text. c) Illustration of single NPL measurements with rotating polarization of the excitation light (light blue) and straight excitation (0 °) along with corresponding intensity variation experimentally observed.

2300027 (5 of 11)

**ADVANCED
SCIENCE NEWS**

www.advancedsciencenews.com

{M} acro-
olecular
Materials and Engineering
Open Access

www.mame-journal.de

orientation (Figure 3b). If the NPLs would have been randomly oriented within the fibers, no difference in the detected intensity would be expected with excitation as well as emission polarization either parallel ($I_{\parallel}$) or perpendicular ($I_{\perp}$) to the fiber direction, that is $I_{\parallel} = I_{\perp}$. If the NPLs would have been aligned parallel to the fiber direction, the intensity observed with excitation and detection polarizations parallel to the fibers should be higher than with polarizations perpendicular to them, $I_{\parallel} > I_{\perp}$. However, in our case, the intensity with polarizations perpendicular to the fibers is about 30% higher than that with polarizations parallel to the fibers, $I_{\parallel} < I_{\perp}$, as expected for NPL orientations perpendicular to the fiber direction.

As mentioned in the introduction, differently oriented NPLs do not only display differences in the polarization of emission and excitation probabilities, but also in their radiation pattern (blue dumbbell in Figure 1i). This can be detected by 3D-photogoniometry (Figure 3c). For this purpose, the fiber was fixed behind a glass hemisphere and excited with a circularly polarized laser (green in Figure 3c). The emission intensity of fibers embedded in refractive index matching materials was measured at different angles along the hemisphere (along the blue and red lines on the hemisphere in Figure 3c). An asymmetric radiation pattern is observed along the blue line while a symmetric radiation pattern is observed along the red line, that runs around the fiber axis. This means that the experimentally observed radiation pattern is matching an emission pattern that is expected when the NPLs lie in the plane of the red line (compare also with Figure 1i) – with minor deviations caused by the slight angular broadening already shown in Figures 2i and 3a – and thus also confirm an orientation perpendicular to the fiber direction.

In the 3D-single particle excitation polarization microscopy, polarized emission spectroscopy and 3D-photogoniometry experiments described above (Figure 2e–i, 3a–c), the fibers were always embedded in refractive index matching materials to observe only the pure signals from the NPLs without any refracting or waveguiding effects at the surfaces of the fibers. However, we also tested the radiation pattern of the aligned NPL emission exciting the electrospun fibers without embedding in refractive index matching materials. As expected for highly aligned orientation of the NPLs perpendicular to the fiber axis and the very smooth fiber surfaces obtained in our SEJS-method, the emission pattern of the light exciting the fibers was indeed confined to a very narrow angle range of about +/- 7–8 ° (Figure 3d).

Finally, to explore the potential presence of aggregated NPLs we performed SAXS measurements (Figure 3e). Several hours of SAXS signal accumulation time was necessary to observe any specific signal from the NPL containing SEJS-fibres (red and

black curves) at all that would indicate any periodically scattering structures such as aggregates. With the same set-up, typically only several minutes are necessary to observe signals from samples that contain periodic heavy atom structures. The weak signals appear to indicate periodically scattering structures at distances of ≈5 nm. While 5 nm corresponds well with the expected distance of stacked NPLs in aggregates[26] the observation time necessary to observe any signal at all demonstrates that only traces of NPLs were aggregated. The red and black SAXS data stem from fibers with NPL concentrations used for the measurements shown in Figures 2, 3a, and 3b–d, respectively. Particularly, aggregation signals from fibers such as used for the data in Figures 2, 3a (red) were only marginally visible in comparison to data from a control fiber without NPLs (blue) even after the very long data accumulation time. Thus, NPL aggregation in these samples is negligible.

3. Discussion

The observed orientations of the NPLs perpendicular to the fiber axis is highly beneficial for numerous optical applications. For example, the vast majority of the photons emitted perpendicularly to the NPLs surface planes stay within the fibers by waveguiding (Figure 3d). This can be used to direct the light specifically into any desired direction even if the light initially absorbed by the NPLs was entirely diffusive or scattered. Also, stimulated emission probabilities are significantly enhanced when all transition dipole moments are oriented perpendicular to a fibers waveguiding direction.

However, the perpendicular orientation of the NPLs observed in the electrospun fibers is also counter-intuitive and raises the question about its origins. In the electrospinning process there are several different forces that might be responsible for the orientation: (i) the flow of the polymer solution in the spinneret (ii) viscoelastic forces within the polymer solution (iii) the electrical field in the spinning process (iv) drawing of the fibers (**Figure 4**).

Strong electric fields can orient aggregated CdSe NPLs. For example, Yoon et al. applied a field of 100 V per 3 μm (3.3×10^7 V m^{-1}), resulting in an orientation of aggregated platelets with the long axis of the platelets along the field.[5] However, in the electrospinning process here a potential of 35 kV is applied over a distance of 40 cm, i.e., field of only $8,75 \times 10^4$ V m^{-1} and with that much lower than the field used by Yoon et al. Furthermore, in the case of electrospinning the electrical field should – similarly as in the case of the aggregated platelets – orient the NPLs along the long axis in spinning direction. However, a

---

d) Optical emission microscope images of individual NPLs oriented as illustrated in (a). e) Illustration of NPLs oriented perpendicular to the fibers direction. f) Intensity variations from a single NPL in electrospun fibers (encircled in h) observed with rotating polarization of the excitation light and excitation from three different directions tilted by 35° (black) along with corresponding fits (red). With excitation perpendicular to the fiber (left), signals highest with polarization perpendicular to the fibers whereas it was lowest when it was parallel (as illustrated by the double arrows on the left), thereby demonstrating perpendicular alignment of the NPLs in the fibers. g) Normalized signals from 19 of 20 individual NPLs had nearly identical phases demonstrating perpendicular orientations h) Optical emission microscopy images of individual NPLs (0.03 wt.%) in the electrospun fibers. Note the darker region in the middle of the fiber originating from its dog-bone like shape (see Figure 1b and Figure 2, Supporting Information). i) Polar plot of the histogram of all orientations observed from NPLs in fibers (projection of the 3D orientations onto the plane parallel to the microscope objectives surface). Average orientation of the NPLs in the x-y plane was 83±21° (red line) with a fiber orientation of −5° (blue line). (Data shown in (b) and (c) are a repetition of three periods from the average of ten rotations of the excitation polarization, resp., due to lower modulation amplitudes from single NPLs parallel to the microscope (b,c). Raw data are shown in Figure 3, Supporting Information.)
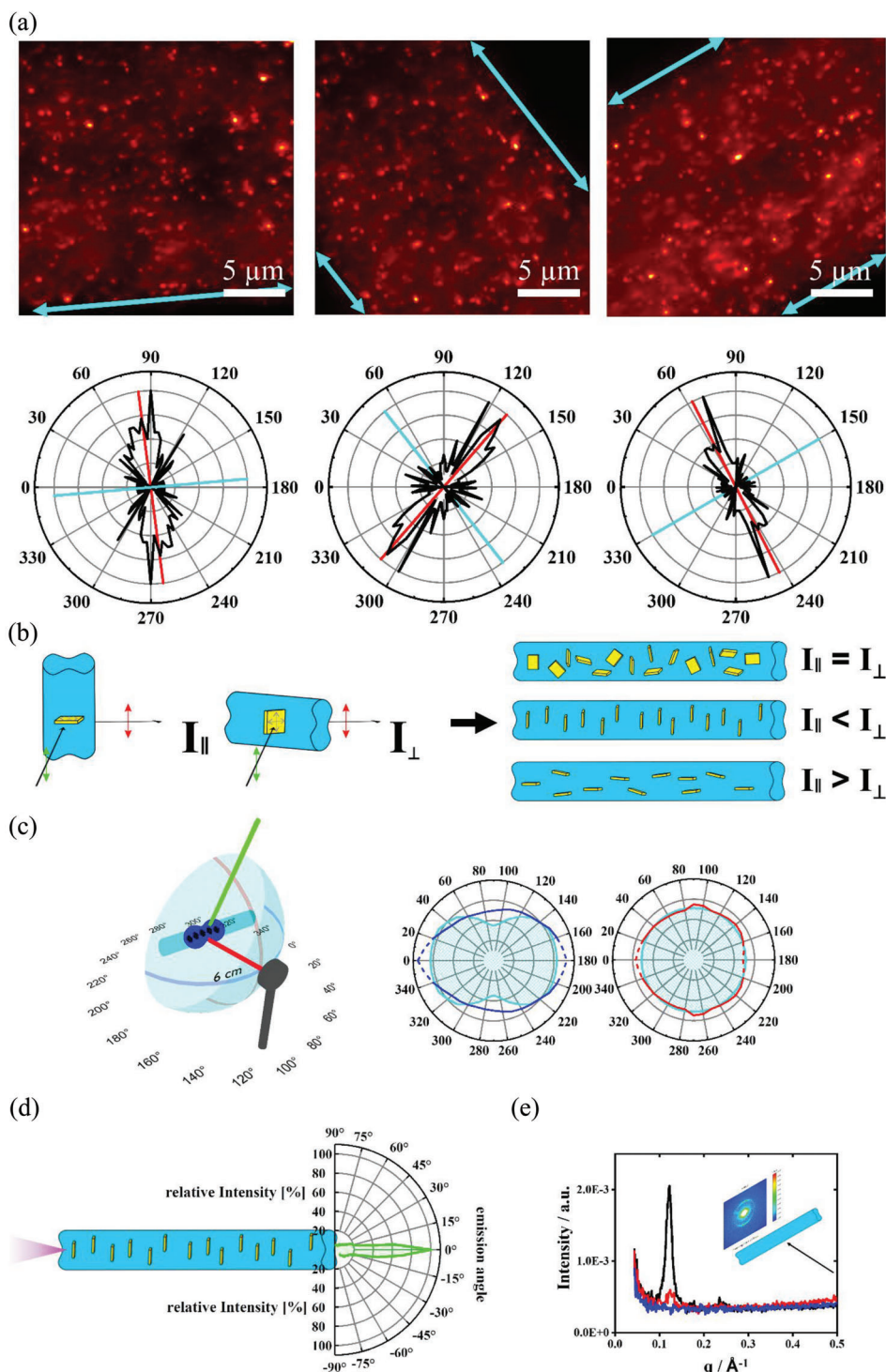
**ADVANCED
SCIENCE NEWS**

www.advancedsciencenews.com

[M] acro-
olecular
Materials and Engineering
Open Access

www.mame-journal.de

Figure 3. a) Optical emission microscopy images and polar plot histograms (black) of single NPL 3D-orientations in electrospun fibers with orientations of 5°, 52°, and 150° (blue lines) confirm on average (red lines) perpendicular NPL alignment . b) Illustration of emission intensity measurements with excitation and emission polarization, parallel ($I_\parallel$) or perpendicular ($I_\perp$) to the fiber direction. The higher intensity observed with polarizations perpendicular to the fiber than parallel to it, $I_\parallel < I_\perp$, confirm perpendicular NPLs orientations . c) Radiation pattern detected by 3D-photogoniometry . The symmetrical radiation pattern perpendicular to the fibers (red lines) and asymmetric radiation pattern parallel to fibers (blue lines) confirms NPL orientations perpendicular to the fiber orientations (compare also with Figure 1i). d) Fiber radiation patterns when not embedded in refractive index matching materials, as was done for measuring the original NPL emissions in Figures 2 and 3a–c (for details see text). e) SAXS measurements confirm that at concentrations used to align the NPLs in the electrospun fibers aggregation is negligible (for details see text, inset is only to illustrate how the fibers were oriented in the SAXS apparatus).
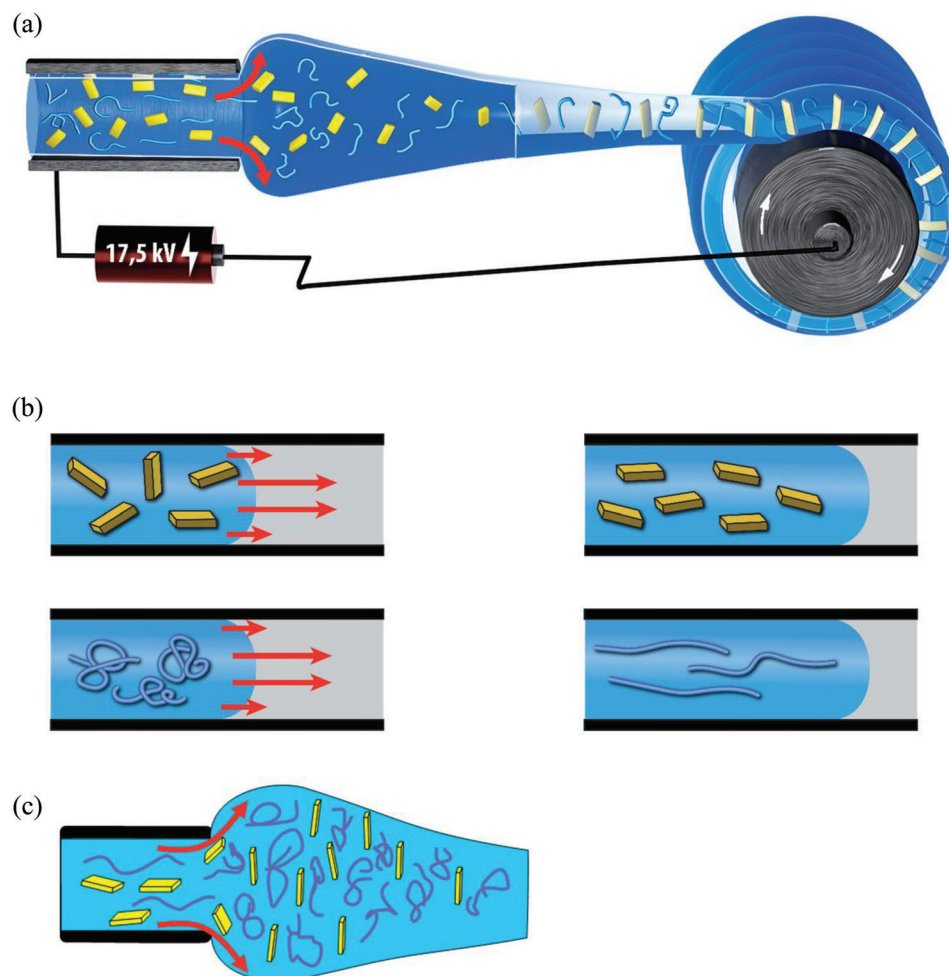
Figure 4. a) Schematic illustration of the proposed processes involved in the counterintuitive perpendicular alignment of the NPLs in electrospun fibers. b) The NPLs in the cannula are initially aligned along the direction of flow, and the polymer chains are stretched in the same direction. c) When exiting the tip, the compressed polymer chains regain a portion of its former shape again resulting in forces acting perpendicularly to the fiber spinning and orienting the NPLs between the polymer chains accordingly. This alignment persists in further process steps during drying of the fiber and on the fiber trajectory to the target. Obviously, any potential final stretching of the fibers due to "pulling" forces at the rotating collector does also not exist. Such stretching could potentially realign the platelets parallel to the fibers but as synchronization of the rotating speed of the collector with the flight speed of the fiber is absolutely essential they do obviously play no role in the final steps of the overall process.

perpendicular orientation is observed. Thus, the alignment due to the electric fields applied in the electrospinning process is very unlikely.[5]

Conventional electrospinning processes comprise the formation of a Taylor cone and ejection of a jet from it.[42] Then, there is a strong drawing of the polymer fibers in the jet after leaving the Taylor cone due to the bending instabilities and resulting chaotic whipping of the jet.[30] However, because there is no such chaotic whipping taking place in the case of the stable jet electrospinning used here, the drawing ratio for the jet is much smaller. Therefore, the change of the NPL orientation due to this part of process is likewise unlikely.

Within the cannula used as spinneret, there is a flow of the non-Newtonian polymer solution that is expected to exert shear forces on both the NPLs as well as the polymer coils. As a laminar flow profile can be assumed within the spinneret, the shear forces result from the fact that the flow velocity is zero at the wall,

but has a maximum in the middle of the tube. These shear forces within the spinneret should orient the NPLs parallel to the flow direction (Figure 4b). Furthermore, the flow will stretch and elongate the polymer coils in the direction of the flow (lower part of Figure 4b).

However, when the polymer solution leaves the cannula, the wall is no longer present and therefore the shear forces cease. The stretched but still entangled polymer chains will then return to the coiled conformation in order to maximize entropy. The recoiling results in a normal force and a swell of the extrudate.

The viscoelastic phenomenon occurring at the exit of the cannula is known as "die swell" or Barus effect in polymer processing.[43,44] We propose that these normal forces are the main forces for the perpendicular orientation of the NPLs (Figure 4c) as the polymer and embedded NPLs emerge from the cannula. The following steps in the fiber formation process are the eruption of a jet from the droplet at the end of the cannula

ADVANCED
SCIENCE NEWS

www.advancedsciencenews.com

Macro-
molecular
Materials and Engineering

www.mame-journal.de

due to the applied electrical field and the drying of the fiber on its trajectory to the target. Since there are no walls, shear forces do not occur and the orientation of the nanoplatelets is maintained as the jet is formed and the resulting fiber dries (Figure 4a).

A controlled reorientation of nano-objects due to such processes is not only of high relevance for the beneficial alignment of emissive 2D NPLs but will open a much larger range of possibilities in the orientating of nanostructures when forces from flows and viscoelasticity of polymer solutions are cleverly designed.

4. Conclusion

In summary, we propose that the alignment of the NPLs is based on the normal forces at the exit of the cannula when the polymers return to their maximum entropy coiled conformation. This alignment persists in further process steps during drying of the fiber and on the fiber trajectory to the target (Figure 4a). Other potential forces that are resulting from the flow of the polymer solution in the spinneret, the electrical field in the spinning process or drawing of the fibers during the formation of the jet from the Taylor cone are either too weak or would result in exactly opposite orientations than the experimentally observed perpendicular ones. The possibility of such counterintuitive alignment of nanoobjects by clever design of the flows, restrictive wall forces and viscoelastic properties will be highly useful for many more applications beyond the alignment of emissive 2D NPLs and future studies are needed to shed more light on the intriguing mechanisms responsible for this unexpected experimental observation. We expect that the principal possibility of orientational forces perpendicular to the flow direction will even allow any desired orientation between parallel and perpendicular using the corresponding microfluidics.

In any case, the practical implications of the observation of perpendicular electrospinning NPL alignment in SJES fibers are quite straightforward. For fiber lasers, highly stable and emissive NPLs oriented perpendicular to the fibers will allow particular high laser amplification and also improvement of signal amplification in telecommunication. Highly emissive NPLs perpendicular to the fiber direction will also be very beneficial for luminescent light concentrator schemes that are intended to collect diffusively scattered light and direct it onto photovoltaics. The predominant emission parallel to the fiber axis will minimize typical escape cone losses, which intrinsically occur in conventional luminescent light concentrators due to emission angles not suitable for wave guiding. Directed light from stable nanoemitters will also be beneficial in the field of display technology, as it avoids the usual loss of light energy emitted into unfavorable directions. Also, entirely new optological schemes will become possible, for example, by combining or redirecting photon streams from and into distinct directions. 2D NPLs with highest emission efficiencies parallel to fibers of high transparencies also raise interesting fundamental questions on the limits of refocusing scattered light into very distinct directions and will also allow to explore these limits. Such a refocusing of diffusively scattered light is clearly impossible with conventional ray optics.

5. Experimental Section

Chemicals: Sodium myristate (≥99%), methanol (MeOH, ≥99.8%), 1-octadecene (ODE, 90%), sulfur (99.98%), n-hexane (≥99%), 2-butanone (>99%) and ethanol (EtOH, ≥99.8%) were supplied from Sigma Aldrich. Cadmium nitrate tetrahydrate (99.999%), selenium (99.999%, 200 mesh) and oleic acid (HOA, 90%) were supplied by Alfa Aesar. Cadmium acetate dihydrate ($Cd(Ac)_2$, 98%) and tri-n-octylphosphine (TOP, 97%) were purchased from ABCR. PMMA was purchased from Röhm (Plexiglas 8N). All chemicals except ODE were used as received without further purification. ODE applied for the preparation of the chalcogenide precursor solutions was obtained by degassing at 120 °C in vacuum ($p \leq 1 \times 10^{-3}$ mbar) for at least 6 h. Afterward, the purified ODE was stored in an air-free glove box.

Synthesis of CdSe Core NPLs: The synthesis of 4 mL CdSe NPLs was performed according to literature procedures.[45] Cadmium myristate ($Cd(myr)_2$ was prepared according to Tessier et al.[36] In brief: In a three-neck flask, 96 mg Se and 1360 mg $Cd(myr)_2$ were mixed in 120 mL ODE and degassed under vacuum (1×10^{-3} mbar) for 60 min at 70 °C, before heating the dispersion to 240 °C under Ar atmosphere. At 205 °C, 240 mg of $Cd(Ac)_2$ were added and the synthesis was kept at 240 °C for 12 min, before it was quenched by the addition of 8 mL HOA and cooling down to room temperature. The NPLs were precipitated by the addition of 40 mL of a 2:1 mixture of EtOH and hexane and centrifuged at 4000 rcf for 10 min. The yellow NPLs were redispersed in 10 mL of hexane. This washing step can be repeated until the supernatant is colorless.

Synthesis of CdSe/CdS Core-Crown NPLs: The growth of a lateral CdS crown around the CdSe core NPLs was achieved according to Schlosser et al.[46] In a three-neck flask, 1.165 mL of CdSe NPLs ($c_{Cd} = 40.0$ mм, $\beta_{CdSe} = 7.64$ mg mL^{-1}) were dispersed in a mixture of 180 µl HOA, 96 mL $Cd(Ac)_2$ and 8 mL ODE. The hexane was removed carefully by vacuum and the mixture was degassed for additional 1 h at 60 °C. Then, the dispersion was heated to 240 °C under an Ar atmosphere. At 215 °C, 6 mL of 0.05 м sulfur-solution in ODE was injected at a rate of 18 mL h^{-1}, while the mixture was continuously heated to 240 °C. After the addition is completed, the dispersion was kept at 240 °C for additional 10 min before rapidly cooling down to room temperature. 10 mL of a 2:1 mixture of EtOH and hexane was added and the dispersion centrifuged at 4000 rcf for 10 min, and the CdSe/CdS core-crown NPLs were redispersed in 2 mL of 2-butanone.

Preparation of Spinning Solution and Electrospinning Process: An NPL in 2-butanone solution from the previous step was first sonicated to help redispersing the NPLs. Then, the spinning solution preparation and fiber fabrication process were performed following the standard SJES parameters based on Christ, Ang et al.[34] Briefly, a spinning solution was prepared by dissolving PMMA (Plexiglas 8N, RÖHM) in the previously prepared NPLs-butanone solutions and stirred for 24 h. Finally, homogenous and yellow solutions were obtained with a PMMA concentration of 35 wt.% and an NPLs concentration of 0.3, 0.03, 0.003 wt.% (with respect to PMMA). The entire procedure was done at room temperatures and humidities. For single particle measurements a concentration of 0.03 wt.% was used to be able to dissect individual particles in the optical microscope. The molecular weight of the PMMA is 83000 g mol^{-1} determined by GPC in THF with calibration using polystyrene standards.

For the fabrication of NPLs doped PMMA fibers, a custom-made electrospinning apparatus was used. Briefly, a 5 mL syringe was filled with a PMMA-NPLs solution and was attached to a metal needle with an inner diameter of 0.51 mm. Subsequently, the electrospinning process was run with parameters as follows: applied voltage = 17.5 kV at metal needle and −17.5 kV at collector, flow rate = 20 mL h^{-1} and tip-to-collector distance = 40 cm. Electrospun microfibers were deposited on a rotating drum metal collector (drum diameter = 100 mm, rotational speed = 2000 rpm) covered with aluminum foil. The environmental conditions (temperature and relative humidity) were kept constant during the whole electrospinning process. The morphology of the obtained fibers was observed with a scanning electron microscope (Evo LS 25, CARL ZEISS).

Preparation of NPLs Monolayer: The monolayer of NPLs on a microscope coverslip was prepared by a layer-by-layer (LbL) deposition process using a dip robot (DR-3, Riegler & Kirstein) as described by Li, Klepzig et al.[41] Since the LbL process is based on electrostatic attraction between

two oppositely charged molecules in aqueous conditions, NPLs were first transferred to aqueous phase via a ligand exchange approach. For this, 11-mercaptoundecanoic acid (MUA) was used to replace oleic acid ligands on NPLs surface, in order to make the NPLs hydrophilic and capable of being deprotonated. Then the NPLs aqueous solution was diluted to a concentration of 0.001 mg mL^{-1} (pH 10) for further use. Polydiallyldimethylammonium chloride (PDDA) was used here as polycation with a concentration of 1 mg mL^{-1} in purified water. The LbL process was carried out as follows: clean coverslips were first immersed into PDDA solution for 10 min, followed by washing with deionized water for 1 min and drying under nitrogen. Then the samples were dipped in NPLs solution for 10 min, followed by rinsing in water and drying with nitrogen again. NPLs orientation was investigated via an atomic force microscope (XE-100, PARK SYSTEMS).

3D single Molecule Orientation Measurements: For the single molecule measurements, the sample of monolayer NPLs in PDDA with a concentration of 0.001 mg mL^{-1} was prepared as described above, while the sample of fibers with NPLs (0.03 wt.%) were bonded with Canada balsam (Sigma-Aldrich) between cover slips.

The measurements were performed on the 3D single-molecule polarization set up, which has been described previously.[9,10,47,48] Briefly, a 488 nm continuous-wave (CW) laser (sapphire 488-50, Coherent) was used for excitation, and then the beam passed through a half-wave plate (achromatic half-plate, 400–800 nm, Thorlabs) in a motorized rotation stage for a constant rotation of the linearly polarized light. Thereafter, the beam passed two wedge-prisms (4° Beam Deviation, 375—700 nm, Thorlabs) with rotation, which shifted the beam laterally. The generated beam was focused onto the back aperture of the microscope objective (NA = 1.35 oil immersion UPlanApo, 60x, Olympus) and illuminated the sample from three different directions (0°, 120°, and 240°). The emitted light was passed through a dichroic mirror (beam splitter R405/488/561/635, AHF), an emission filter (ET band pass 525/50, AHF) and finally collected by an EMCCD camera (iXonEM+897 back illuminated, Andor Technology).

The power of excitation light was 0.02 mW. 400 frames were recorded in each direction with a frame frequency of 30 Hz (15 frames per period).

The measurements were done with single non-merged fibers. The results were reproduced after a few weeks, i.e., basically no loss in the perpendicular NPL orientation could be observed during a time period of several weeks.

Fluorescence Spectroscopy: The measurements were performed using a Cary Eclipse Fluorescence spectrometer (VARIAN). The sample of fibers with NPLs (0.03 wt.%) were bonded with Canada balsam (Sigma-Aldrich) between cover slips. Fluorescence excitation spectra were taken from vertical and horizontal clamped fibers and polarized excitation scans were performed using vertically or horizontally polarized excitation and detection (Manual Polarizer Accessory from VARIAN).

3D-Photogoniometry: A 485 nm diode laser (PICO-QUANT) was used as a light source to excite the vertical and horizontal clamped fibers containing 0.03 wt.% NPLs. The further setup has been reported previously.[9] However, an excitation filter (FES500, THORLABS) and an emission filter (ET band pass 535/50, AHF) were installed in the path way, as well as a quarter-wave plate to polarize the beam circularly. Furthermore, the laser excitation beam was directed at angles of 39° onto the fibers.

Direct Fiber Radiation Measurements: A bunch of ten fibers with a length of 5 cm was clamped and excited at one end of the bunch with a 405 nm Laser. For this, a Verdi G10 (Coherent) and Vitesse Duo (Coherent) pumped a RegA9000 (Coherent). The resulting 800 nm femtosecond pulses was adjusted to a wavelength of 405 nm using an OPA 9400 (Coherent). The excitation is focused and cleaned up with a 750 nm short-pass filter (FES750, Thorlabs). At the other end of the fibers the emission was measured. A powermeter (LabMax-TOP, Coherent) was used with an emission filter (ET band pass 535/50, AHF) attached to detector. Using a rotational stage, the detector of the powermeter was rotated around the end of the fiber bunch.

SAXS: Small-angle X-ray scattering (SAXS) measurements were performed in transmission mode on a RIGAKU system consisting of a microfocus X-ray tube with Cu target and mirror optics ($\lambda = 1.541$ Å), a three-pinhole collimating system, and a 2D gas-filled multiwire detector

from MOLECULAR METROLOGY. The sample-to-detector distance was 150 mm. The fibers were measured for 2 h.

Supporting Information

Acknowledgements

Conflict of Interest

The authors declare no conflict of interest.

Author Contributions

Conceptualization: H.M., J.L., P.J.W.; Methodology: M.H., X.L., F.L., H.-A.C.; Software: M.H.; Validation: M.H., X.L., F.L.; Formal analysis: M.H., X.L; Investigation: X.L., M.H., F.L., M.M.W., A.S., P.B.; Visualization: M.H., F.L., L.F.K., X.L.; Resources: F.L., L.F.K., H.-A.C.; Data Curation: F.L., M.H., X.L.; Funding acquisition: H.M., J.L., P.J.W.; Project administration: H.M., J.L., P.J.W.; Supervision: H.M., J.L., P.J.W., M.H.; Writing – original draft: M.H., P.J.W.; Writing – review & editing: F.L., H.M., J.L., L.F.K., M.H., P.J.W., X.L.

Data Availability Statement

The data that support the findings of this study are available from the corresponding author upon reasonable request.

Keywords

[1] S. Pedetti, S. Ithurria, H. Heuclin, G. Patriarche, B. Dubertret, *J. Am. Chem. Soc.* **2014**, *136*, 16430.

[2] R. Scott, J. Heckmann, A. V. Prudnikau, A. Antanovich, A. Mikhailov, N. Owschimikow, M. Artemyev, J. I. Climente, U. Woggon, N. B. Grosse, A. W. Achtstein, *Nat. Nanotechnol.* **2017**, *12*, 1155.

**ADVANCED
SCIENCE NEWS**

www.advancedsciencenews.com

**acro-
olecular
Materials and Engineering**
Open Access

www.mame-journal.de

[3] J. S. Son, J. H.o Yu, S. G.u Kwon, J. Lee, J. Joo, T. Hyeon, *Adv. Mater.* **2011**, *23*, 3214.

[4] S. Shendre, S. Delikanli, M. Li, D. Dede, Z. Pan, S. T. Ha, Y. H. Fu, P. L. Hernández-Martínez, J. Yu, O. Erdem, A. I. Kuznetsov, C. Dang, T. C. Sum, H. V. Demir, *Nanoscale* **2019**, *11*, 301.

[5] D. E. Yoon, W. D. Kim, D. Kim, D. Lee, S. Koh, W. K. Bae, D. C. Lee, *J. Phys. Chem. C* **2017**, *121*, 24837.

[6] Y. Gao, M. C. Weidman, W. A. Tisdale, *Nano Lett.* **2017**, *17*, 3837.

[7] P. D. Cunningham, J. B. Souza, I. Fedin, C. She, B. Lee, D. V. Talapin, *ACS Nano* **2016**, *10*, 5769.

[8] B. Abécassis, M. D. Tessier, P. Davidson, B. Dubertret, *Nano Lett.* **2014**, *14*, 710.

[9] A. Pieper, M. Hohgardt, M. Willich, D. A. Gacek, N. Hafi, D. Pfennig, A. Albrecht, P. J. Walla, *Nat. Commun.* **2018**, *9*, 666.

[10] M. M. Willich, L. Wegener, J. Vornweg, M. Hohgardt, J. Nowak, M. Wolter, C. R. Jacob, P. J. Walla, *Proc. Natl. Acad. Sci. USA* **2020**, *117*, 32929.

[11] J. Chun, J. Lee, *Eur. J. Inorg. Chem.* **2010**, *2010*, 4251.

[12] W. U. Huynh, J. J. Dittmer, A. P. Alivisatos, *Science* **2002**, *295*, 2425.

[13] S. Shabahang, S. Kim, S.-H. Yun, *Adv. Funct. Mater.* **2018**, *28*, 1706635.

[14] J. Wang, K. Petermann, *IEEE J. Lightwave Technol.* **1992**, *10*, 96.

[15] B. Guzelturk, M. Pelton, M. Olutas, H. V. Demir, *Nano Lett.* **2019**, *19*, 277.

[16] B. Guzelturk, Y. Kelestemur, M. Olutas, S. Delikanli, H. V. Demir, *ACS Nano* **2014**, *8*, 6599.

[17] J. Guo, M. Niu, C. Yang, *Optica* **2017**, *4*, 1285.

[18] L. Wang, C. Zhong, D. Ke, F. Ye, J. Tu, L. Wang, Y. Lu, *Adv. Opt. Mater.* **2018**, *6*, 1800427.

[19] R. Clausius, *Ann. Phys. Chem.* **1850**, *155*, 368.

[20] J. F. Miethe, A. Schlosser, J. G. Eckert, F. Lübkemann, N. C. Bigall, *J. Mater. Chem. C* **2018**, *6*, 10916.

[21] O. Erdem, K. Gungor, B. Guzelturk, I. Tanriover, M. Sak, M. Olutas, D. Dede, Y. Kelestemur, H. V. Demir, *Nano Lett.* **2019**, *19*, 4297.

[22] B. Guzelturk, O. Erdem, M. Olutas, Y. Kelestemur, H. V. Demir, *ACS Nano* **2014**, *8*, 12524.

[23] A. Antanovich, A. Prudnikau, A. Matsukovich, A. Achtstein, M. Artemyev, *J. Phys. Chem. C* **2016**, *120*, 5764.

[24] R. Momper, H. Zhang, S. Chen, H. Halim, E. Johannes, S. Yordanov, D. Braga, B. Blülle, D. Doblas, T. Kraus, M. Bonn, H. I. Wang, A. Riedinger, *Nano Lett.* **2020**, *20*, 4102.

[25] O. Erdem, M. Olutas, B. Guzelturk, Y. Kelestemur, H. V. Demir, *J. Phys. Chem. Lett.* **2016**, *7*, 548.

[26] S. Jana, T. N. T. Phan, C. Bouet, M. D. Tessier, P. Davidson, B. Dubertret, B. Abécassis, *Langmuir* **2015**, *31*, 10532.

[27] L. A. Bosworth, S. Downes, *Electrospinning for tissue regeneration*, Woodhead Pub, Oxford, Cambridge **2011**.

[28] A. Greiner, J. H. Wendorff, *Angew. Chem., Int. Ed. Engl.* **2007**, *46*, 5670.

[29] S. Jian, J. Zhu, S. Jiang, S. Chen, H. Fang, Y. Song, G. Duan, Y. Zhang, H. Hou, *RSC Adv.* **2018**, *8*, 4794.

[30] R. Dukali, I. Radovic, D. Stojanovic, D. Sevic, V. Radojevic, D. Jocic, R. Aleksic, *J. Serb. Chem. Soc.* **2014**, *79*, 867.

[31] N. Tomczak, S. Gu, M. Han, N. F. Van Hulst, G. Julius Vancso, *Eur. Polym. J.* **2006**, *42*, 2205.

[32] L. A. Carnell, E. J. Siochi, N. M. Holloway, R. M. Stephens, C. Rhim, L. E. Niklason, R. L. Clark, *Macromolecules* **2008**, *41*, 5345.

[33] Y. Z. Zhang, B. Su, S. Ramakrishna, C. T. Lim, *Biomacromolecules* **2008**, *9*, 136.

[34] H.-A. Christ, P. Y. Ang, F. Li, H.-H. Johannes, W. Kowalsky, H. Menzel, *J. Polym. Sci.* **2022**, *60*, 715.

[35] H. Yuan, S. Zhao, H. Tu, B. Li, Q. Li, B. Feng, H. Peng, Y. Zhang, *J. Mater. Chem.* **2012**, *22*, 19634.

[36] M. D. Tessier, P. Spinicelli, D. Dupont, G. Patriarche, S. Ithurria, B. Dubertret, *Nano Lett.* **2014**, *14*, 207.

[37] D. Han, L. Yang, Z. Hu, Z. Du, Y. Wang, Z.e Yuan, Q. Wang, M. Artemyev, J. Tang, *ScienceAsia* **2020**, *46*, 595.

[38] Q. Zhou, M. Bao, H. Yuan, S. Zhao, W. Dong, Y. Zhang, *Polymer* **2013**, *54*, 6867.

[39] B. Akinalan Balik, S. Argin, *J. Appl. Polym. Sci.* **2020**, *137*, 48294.

[40] L.u Li, Z. Jiang, M. Li, R. Li, T. Fang, *RSC Adv.* **2014**, *4*, 52973.

[41] F. Li, L. F. Klepzig, N. Keppler, N. C. Bigall, H. Menzel, J. Lauth, *Langmuir* **2022**, *38*, 11149.

[42] G. I. Taylor, *Proc. R. Soc. Lond. A* **1964**, *280*, 383.

[43] T. G. Mezger, *The Rheology Handbook: For users of rotational and oscillatory rheometers*, Vincentz Network, Hanover, Germany **2020**.

[44] M. Trebbin, D. Steinhauser, J. Perlich, A. Buffet, S. V. Roth, W. Zimmermann, J. Thiele, S. Förster, *Proc. Natl. Acad. Sci. U.S.A.* **2013**, *110*, 6706.

[45] S. Ithurria, M. D. Tessier, B. Mahler, R. P. S. M. Lobo, B. Dubertret, A.l. L. Efros, *Nat. Mater.* **2011**, *10*, 936.

[46] A. Schlosser, R. T. Graf, N. C. Bigall, *Nanoscale Adv* **2020**, *2*, 4604.

[47] D. Pfennig, A. Albrecht, J. Nowak, P. J. Walla, *Chem. Phys.* **2020**, *538*, 110853.

[48] M. Hohgardt, F. E. Gädeke, L. Wegener, P. J. Walla, *Polymers* **2022**, *14*, 532.